THREE SPECIMEN GEOMETRIES AND THREE METHODS
OF DATA EVALUATION IN SINGLE-FIBER PULLOUT TESTS

S. Zhandarov,[1,2] C. Scheffler,[1*] E. Mäder,[1] and U. Gohs[1]

Keywords: *fiber-matrix interface, microbond test, pullout test, local interfacial shear strength, interfacial frictional stress*

The shapes of force–displacement curves recorded in single-fiber pullout and microbond tests are analyzed within the framework of a stress-based model of interfacial debonding. Three characteristic points allowing one to evaluate the local interfacial strength parameters, the local interfacial shear strength (IFSS), and the interfacial frictional stress, using several different methods, can be marked out in each curve. The "alternative" method based on the measured peak force and initial postdebonding force appeared to be more reliable than the "traditional" one using the debond force for calculating the local IFSS in fiber–matrix systems. The effect of specimen geometry on force–displacement curves and on calculated local interfacial strength parameters was investigated. Though the "equivalent cylinder" approximation often yields a good estimate of these parameters, there is a need for a method which would explicitly include the actual specimen geometry.

Introduction

Though the fiber pullout from a matrix as a means of estimating the interfacial bond strength in fiber–matrix systems was first proposed more than 50 years ago [1], the pullout techniques (microbond [2] and pullout [3] tests) still remain the most popular methods for determining the interfacial strength parameters in fiber-reinforced composites. This is explained, in particular, by their versatility. These techniques can successfully be used for a very wide range of fiber–matrix systems — combinations of glass, carbon, polymer, natural, metal, and other fibers with polymer (both thermoplastic and thermosetting), metal, ceramic, and concrete matrices [2-10]. Over the years, a considerable progress has been made in the practical aspects of pullout experiments and in the methods of data reduction. Nevertheless, most of the researchers using pullout techniques

[1]Leibniz-Institut für Polymerforschung Dresden e.V., Hohe Strasse 6, D-01069 Dresden, Germany
[2]V. A. Bely Metal-Polymer Research Institute, National Academy of Sciences of Belarus, Kirov Str. 32a, 246050 Gomel, Belarus
[*]Corresponding author; tel.: +49 351 4658345; fax: +49 351 4658362; e-mail: scheffler@ipfdd.de

still limit themselves, in the old way, solely to calculations of the mean (apparent) interfacial shear strength (IFSS) between the fiber and matrix. However, an analysis of the force–displacement curves obtained in pullout and microbond tests can yield much more information, and, what is more, information which characterizes fiber–matrix interfacial strength properties more adequately. The aim of this paper is to compare different treatment methods of experimental force–displacement curves for specimens having different geometrical shapes.

1. Theoretical Consideration

1.1. Interfacial crack propagation and the factors controlling it

The main reason for the wide use of pullout techniques is even not their universality, but, to a greater degree, the fact that they are direct and simple in experiments. In pullout and microbond tests, a single fiber is pulled out of a matrix droplet or block in which it has been preliminary embedded, and the force–displacement curve is recorded (or, in some cases, only the peak force is measured). Traditionally, the interfacial bond strength between the fiber and matrix is characterized in terms of the apparent (average) interfacial shear strength (IFSS), defined as [2]

$$\tau_{app} = \frac{F_{max}}{A_f l_e} \, , \tag{1}$$

where F_{max} is the peak force required for complete fiber pullout, A_f is the perimeter of fiber cross section, and l_e is the embedded fiber length. Most of researchers limit themselves to this equation, ignoring the fact that τ_{app} characterizes the interfacial bond (adhesional) strength only indirectly. The interfacial shear stress is constant along the embedded fiber length only if the matrix is purely plastic [11]; in all other cases, the interface includes segments where the shear stress is greater or smaller than its mean value given by Eq. (1). Moreover, numerous experiments on a wide variety of fiber–matrix systems [12-16] have shown that τ_{app} strongly depends on the embedded length l_e and therefore cannot be used as a true interfacial strength parameter, which should not depend on the interface and specimen geometry. And, finally, direct observations [17-21] and analyses of force–displacement curves [22-24] clearly demonstrated that fiber debonding from the matrix during the pullout process occurs through interfacial crack propagation, and the measured force includes contributions from both the adhesional bonding in the intact interface segments and the interfacial friction in already debonded regions. In particular, at the moment when the force is at its maximum, both the interfacial adhesion and the friction contribute to this peak value. Moreover, a variation in the embedded length changes not only the resulting value of τ_{app}, but also the ratio between the adhesional and frictional parts in it. At larger embedded lengths, the frictional contribution can even prevail over the adhesional one [25]. Thus it becomes obvious that the use of τ_{app} as a measure of the interfacial bond strength is, to a high degree, conventional and, strictly speaking, incorrect.

In order to find a more adequate measure of the interfacial bond strength in fiber–matrix systems and to get more information from the raw data obtained in pullout and microbond tests, we have to theoretically consider the processes of initiation and propagation of interfacial crack. This can be done using either of the two approaches, differing by the criterion of interfacial failure accepted, both of them including a large number of specific theoretical models. In the first one (stress-controlled debonding [12, 13, 25-30]), the local IFSS τ_d, i.e., to a first approximation, the local interfacial shear stress near the crack tip is considered as the failure criterion. In the second approach, which is based on fracture mechanics, the failure criterion is the critical energy release rate G_{ic} (energy-controlled debonding [13, 17, 31-35]). Both approaches assume that the corresponding critical quantity (τ_d or G_{ic}) is constant during the whole pullout process; the aim is to determine this value from experimental data. As has been shown in [36, 37], the stress-controlled and energy-controlled debonding approaches are complementary and do not contradict to each other. In this paper, we will use the stress-based model developed by Zhandarov and Mäder, whose most detailed description can be found in [15].
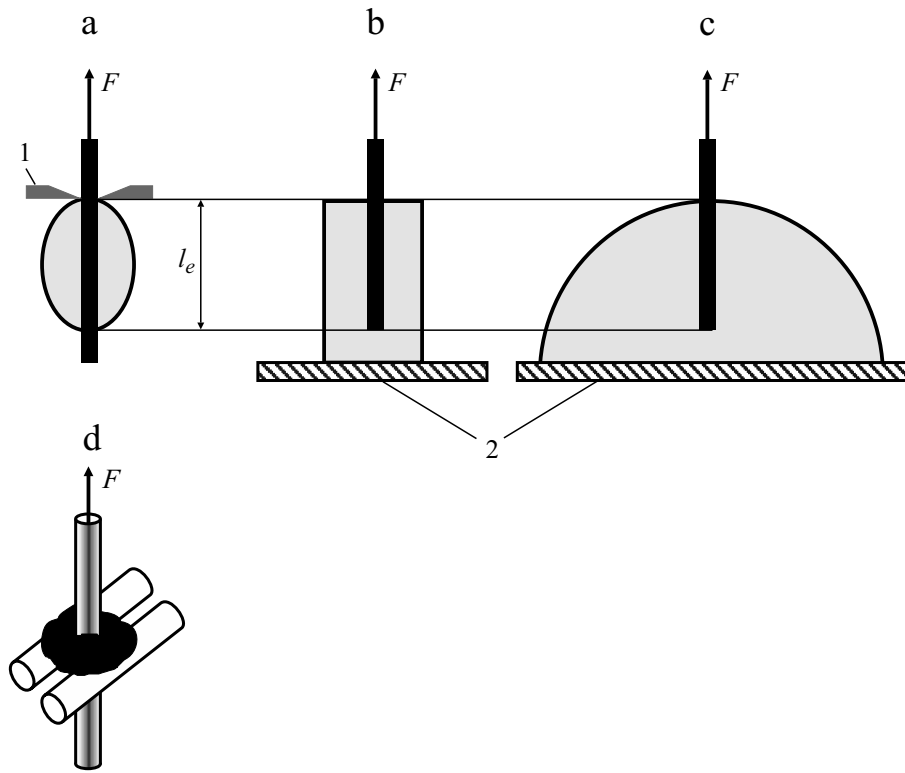
Fig. 1. Specimen geometries used in microbond and pullout tests: ellipsoidal (a), cylindrical (b), spherical segment (c), and "three-fiber method" specimen (d).

1.2. Possible specimen shapes in pullout and microbond tests

From general considerations, it is obvious that the interfacial crack propagation should depend on the geometrical shape of specimen and the loading pattern. The specimen shapes used most often are presented in Fig. 1. First of all, we should note that pullout test and microbond tests do not differ by specimen shape, size, or preparation method, as is often erroneously believed, but solely by boundary conditions: in the microbond test, fixed is the "front" (close to the loaded fiber end) part of the matrix (Fig. 1a), but in the pullout test — its "rear" part (Fig. 1b, c). The force–displacement curves from these two tests are very similar, and, in stress-based analyses, the difference between the pullout and microbond tests can often be neglected [38]. In the microbond test, practically the only available specimen type is an approximately ellipsoidal microdroplet sitting on the fiber, with eventual menisci at both droplet sides. On the contrary, the matrix "droplets" in the pullout test are much more diverse: a cylinder [12, 17, 39], a spherical segment [24, 40, 41], a prism (in particular, a rectangular parallelepiped [42]), a thin disc in which the fiber runs parallel to the base plane [18, 43, 44], etc. As a curious case, we can mention the "three-fiber" test [45] (Fig. 1d), in which the matrix droplet is held by two parallel thick fibers perpendicular to the fiber investigated. The specimen shape in this test is extremely intricate for analysis, and the three-fiber test, strictly speaking, is neither of microbond nor pullout type. In the further analysis, we will consider only three most popular specimens — a cylinder, a spherical segment, and an ellipsoid, ignoring the menisci at fiber entry points.
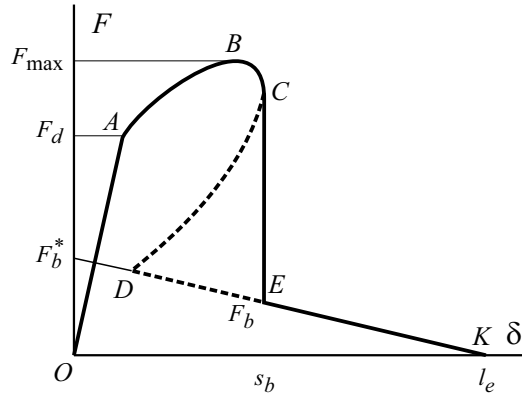
Fig. 2. Idealized force–displacement curve F–δ in the pullout test (for details, see Subsect. 1.3).

1.3. Important points in force–displacement curves

The shape of a typical force–displacement curve in the pullout test (Fig. 2) is governed by the process of interfacial crack propagation. While the whole interface remains intact, the applied load is practically proportional to the displacement of the grip with the fiber in it (segment OA). At this, first stage, the slope of the plot is determined by the compliance of the experimental installation, including the specimen. At the point A, the external force reaches its critical value (F_d, debond force), and an interfacial crack is initiated — the fiber begins to debond from the matrix [17, 22]. However, at first, the measured force continues to increase with crack growth, because the total frictional force in debonded regions is nearly proportional to the crack length, while the adhesional force in the intact segment decreases initially not so fast, though with a steadily increasing rate. Therefore, the force–displacement plot begins to deviate from a straight line, and at the point A, a more or less distinct 'kink' is observed. At the point B, these two rates become equal, and the adhesional force decreases faster than the frictional force increases; thus, the point B corresponds to the peak force ($F = F_{max}$). The segment BC, where the applied force decreases steadily is, as a rule, very short; at the point C, a further crack growth would cause a simultaneous decrease in both the force F and the displacement s (segment CD). However, the tensile testing machines are usually constructed in such a way that their movable grip cannot change its movement direction during the test. As a result, the segment CD is experimentally unobservable, and at $s = s_b$, instantaneous ("catastrophic") debonding of the remaining part of fiber occurs [46]. The registered force drops to F_b at a point E, and the last segment of the curve is fully determined by friction between the debonded fiber and the channel within the matrix. As the fiber is being pulled out, the frictional force decreases in accord with the length of its part remaining in the matrix and reaches zero at the complete pullout ($s = l_e$). (In the microbond test, the matrix droplet as a whole slides along the fiber, and the force applied to the right of the point E remains constant and equal to F_b).

Thus, the force–displacement curve includes three characteristic points corresponding to the changes in the process of interfacial crack propagation:

- F_d — the debond force (crack initiation);
- F_{max} — the maximum force (change the balance of adhesional and frictional contributions);
- F_b — the initial frictional force (complete debonding).

In addition, the coordinate of the point K ($s = l_e$) indicates the embedded fiber length. Since the slope of the segment EK is usually very small, the value of l_e may contain a considerable error, and it is recommended to check it by other means. In the microbond test, the embedded length is measured directly using an optical microscope.

The values of F_d, F_{max}, and F_b form a basis for calculating the interfacial strength parameters for a given individual specimen.

1.4. Model

The model assumed in this paper, as many other stress-based models, is based on the one-dimensional shear-lag stress transfer method originally proposed by Cox [47], but with a corrected shear-lag parameter introduced by Nayfeh [48], which has been proved by Nairn et al. [17, 35, 49] to be more adequate for single-fiber composites than the Cox model. Our analysis includes the residual thermal stresses and the interfacial friction in debonded regions. The main assumptions of this model are as follows:

- The fiber and matrix are purely elastic. The matrix is isotropic and the fiber is transversely isotropic.
- The matrix droplet can be considered as a cylinder with an effective radius R_{eff}, which is chosen to match the total matrix volume around the embedded part of fiber (the equivalent cylinder model [35]). The fiber is also assumed to be cylindrical (of radius r_f) and coaxially embedded in the matrix cylinder.
- The friction in the debonded part of the interface is constant, i.e., in terms of the 'interfacial frictional stress' τ_f, we can assume that $\tau_f = \mathrm{const}$.

The last assumption means that the interfacial behavior in debonded regions is not modeled by the Coulomb friction. It follows from experiments that the shear stress in the debond zone is not strictly proportional to the applied load, but is often roughly constant [17, 35, 50]. As has been shown by many researchers [15, 19, 25, 46, 50–53], the force–displacement pullout curves modeled under these assumptions show good agreement with experimental data.

This model was presented in detail in [15, 25, 46], and numerous experiments [19, 51] have demonstrated that it is sufficiently accurate. It includes two independent interfacial parameters: the local IFSS τ_d and the interfacial frictional stress τ_f, which are assumed to be constant for a given specimen, but may vary from one specimen to another. One of our most important results obtained using this model was the relation for the force applied to the loaded fiber end as a function of crack length [15], namely,

$$F(a) = \frac{2\pi r_f}{\beta}\left\{ \tau_d \tanh\left[\beta(l_e - a)\right] - \tau_T \tanh\left[\beta(l_e - a)\right]\tanh\frac{\left[\beta(l_e - a)\right]}{2} + a\beta\tau_f \right\}, \tag{2}$$

where

$$\tau_T = \frac{\beta r_f E_A}{2}(\alpha_A - \alpha_m)\Delta T$$

is a term, having the dimension of stress, that appears due to the residual thermal stresses; E_A is the axial tensile modulus of fiber, α_A is the axial coefficient of thermal expansion (CTE) of fiber, α_m is the axial CTE of matrix, ΔT is the difference between test and stress-free temperatures (which, for polymers, is considered equal to the glass-transition temperature), and β is the shear-lag parameter as defined by Nayfeh [48], namely,

$$\beta^2 = \frac{2}{r_f^2 E_A E_m}\left[\frac{E_A V_f + E_m V_m}{\dfrac{V_m}{4G_A} + \dfrac{1}{2G_m}\left(\dfrac{1}{V_m}\ln\dfrac{1}{V_f} - 1 - \dfrac{V_f}{2} \right)} \right],$$

where E_m is the tensile modulus of matrix, G_A is the longitudinal shear modulus of fiber, G_m is the shear modulus of matrix, and V_f and V_m are the fiber and matrix volume fractions, respectively, in the specimen. It has to be noted that Eq. (2) is valid for both pullout and microbond tests.

Equation (2) can easily be linked to the important points in force–displacement curves. Indeed, $F_d = F(0)$ and $F_b = F(l_e)$. The calculation of $F_{\max}$ requires an additional analysis, which was carried out in [15]. The equation for the peak force has the form

$$F_{\max}\left(l_e\right)=\begin{cases}\dfrac{2\pi r_f}{\beta}\left[\tau_d\tanh\left(\beta l_e\right)-\tau_T\tanh\left(\beta l_e\right)\tanh\left(\dfrac{\beta l_e}{2}\right)\right],\\[2mm]\beta l_e<\ln\left(u+\sqrt{u^2+1}\right),\\[2mm]\dfrac{2\pi r_f}{\beta}\left\{\tau_d\dfrac{u}{\sqrt{u^2+1}}-\tau_T\left(1-\dfrac{1}{\sqrt{u^2+1}}\right)+\tau_f\left[\beta l_e-\ln\left(u+\sqrt{u^2+1}\right)\right]\right\},\\[2mm]\beta l_e\geq\ln\left(u+\sqrt{u^2+1}\right),\end{cases}\tag{3}$$

where

$$u=\frac{\sqrt{\tau_T^2+4\tau_f\left(\tau_d-\tau_f\right)}-\tau_T}{2\tau_f}.\tag{4}$$

1.5. Why has the specimen shape to be taken into account?

Equation (2) implicitly (through the value of β) includes V_f and V_m — the fiber and matrix volume fractions in the specimen. For cylindrical specimens, obviously,

$$V_f=\frac{r_f^2}{R_m^2},$$

where R_m is radius of the matrix cylinder (see Fig. 1b).

For specimens of other geometrical shapes, V_f and V_m can depend on the embedded length l_e. Expressions for V_f in a hemispherical matrix droplet and in an of ellipsoid of revolution are [25]

$$V_f=\frac{r_f^2}{r_f^2+l_e\left(\sqrt{R_m^2-r_f^2}-\dfrac{l_e}{3}\right)}\quad\text{(Fig. 1c)},$$

$$V_f=\frac{3}{1+2\left(R_m/r_f\right)^2}\quad\text{(Fig. 1a)},$$

respectively.

The embedded length does not appear in Eq. (9) explicitly, but is determined implicitly by the droplet radius and ratios between the axes of the matrix ellipsoid. It is advisable to measure both the embedded length and the droplet diameter for each individual specimen. For a theoretical consideration, the Carroll model [54] or the spherical approximation for the droplet shape can be used. As was shown in [55], the approximation of real ellipsoidal droplets by spherical ones (with the same l_e) does not lead to great errors. The fiber volume fraction in a spherical droplet in the microbond test is [25]

$$V_f=\frac{1}{1+\dfrac{l_e^2}{6r_f^2}}.$$

It is considerably (by 2-3 orders of magnitude) greater than that in typical pullout specimens and, in addition, very strongly depends on the embedded length l_e. As can be seen, the final form of Eq. (2) and, consequently, the determined values of τ_d and τ_f, depend on the specimen shape even if the equivalent cylinder approach is used. The fiber volume fractions for other possible specimen shapes can be found by direct calculations.

1.6. Three approaches to the determination of interfacial strength parameters

As was already noted, the model assumed by us includes two independent parameters, τ_d and τ_f. On the other hand, using the force–displacement curve obtained from a pullout or microbond test, three equations involving these parameters can be taken for the specimen tested:

$$F(0) = F_d^{exper}, \tag{5}$$

$$F_{max} = F_{max}^{exper} \text{ (according to Eq. (5)),}$$

$$F(l_e) = F_b^{exper}. \tag{6}$$

Therefore, τ_d and τ_f can be determined using several different approaches.

1.6.1. "Traditional" approach. The local IFSS τ_d is determined from the force F_d corresponding to the "kink" in the force–displacement curve (Eq. (5)). Then, its value is inserted into Eqs. (4) and (3), and the implicit equation obtained is solved for τ_f (e.g., using the iteration method).

This approach was historically the first and appeared before the publication of the model presented in this paper. Since the debond force F_d does not depend on the interfacial friction, the assumption $\tau_f = const$ can be omitted, but then only the local IFSS τ_d can be calculated. This was done by many authors, who did not limit themselves to the determination of τ_{app}, but was not aimed at the estimation of interfacial friction [13, 56-58].

1.6.2. "Alternative" approach. In the real practice, the "kink" at the point *A* in the force–displacement curve often is not distinct. Most often, this is due to the high compliance of the experimental installation, which results from, e.g., a large free fiber length (between the point of its entry into the matrix and the movable grip). Therefore, the debond force F_d can be measured only with a significant error, which, in turn, entails errors in the calculated values of τ_d and especially τ_f. At the same time, the forces F_{max} and F_b are measured reliably enough. This can be the basis for an alternative method of calculation of interfacial strength parameters. First, the interfacial frictional stress τ_f is determined from Eq. (13), whose explicit form is

$$F_b^{exper} = 2\pi r_f l_e \tau_f.$$

Since τ_f is proportional to the slope of the line EK (see Fig. 2), F_b^{exper} should be replaced by F_b^*, the intercept of the line EK on the vertical axis. Then, the calculated value of τ_f is inserted into Eqs. (4) and (3), and the resulting implicit equation is solved for τ_d. Note that a similar method was used in some simple energy-based models for fiber pullout from concrete matrices [32]. In these models, the critical energy release rate G_{ic} appears to depend on the difference $F_{max} - F_b$, but F_d is not involved in the final equation for G_{ic}.

1.6.3. "Indirect" method. This method was developed by Zhandarov et al. [25] for experimentalists whose test installations cannot record force–displacement curves and solely the values of F_{max} are measured. In this case, a large number of specimens in a widest possible range of embedded lengths is tested, and then the nonlinear least squares method with two fitting parameters, τ_d and τ_f, is used to fit the experimental $F_{max}(d)$ relation with the theoretical Eq. (3). The pair of values $\{\tau_d, \tau_f\}$ which minimizes the sum

$$S = \frac{\sum_{i=1}^{n}\left[F_{i\,max}^{exper} - F_{i\,max}^{theor}\left(\tau_d, \tau_f, ...\right)\right]^2}{n-2},$$

where *n* is the number of specimens, is chosen as the best approximation of the local IFSS and the interfacial frictional stress for the given fiber–matrix pair.

1.6.4. A fourth approach. Finally, we should note that one more approach to the calculation of interfacial strength parameters is possible, namely, from the values of F_d and F_b (Eqs. (5) and (6)). Here, the interfacial strength parameters are determined, in a sense, independently. This method has the same disadvantages as the "traditional" one (large errors in the measured F_d and, consequently, in the calculated τ_d), but the values of the interfacial frictional stress are sufficiently accurate.

TABLE 1. Fiber and Matrix Properties and Specimen Dimensions

Property	Fibers		
	Poly(vinyl alcohol)	E-glass	Carbon
Brand name (if applicable) and manufacturer	Kuralon K-II REC15, Kuraray Co. Ltd, Japan	Leibniz-Institut für Polymerforschung, Dresden, Germany	T700SC-12000 Toray Co., Ltd., Japan
Fiber diameter $2r_f$, µm	32-50	16-22	7
Axial tensile modulus E_A, GPa	35	75	230
Axial Poisson's ratio v_A	0.2	0.17	0.2
Axial Poisson's ratio- α_A 10^{-6} K^{-1}	n/a*	5	0.38
Embedded fiber length l_e, µm	500-1500	100-210	40-110

In this paper, we will not consider this approach separately, because the procedures to determine τ_d and the calculated values are the same as in the traditional approach, and the procedures and values for τ_f are the same as in the alternative one.

2. Experimental

2.1. Materials and specimen geometries

In this paper, we used pullout and microbond tests to determine interfacial strength parameters in several fiber-matrix systems.

(1) Poly(vinyl alcohol) fibers + concrete and a cylindrical specimen geometry.

The PVA (Kuralon K-II REC15) fibers used were produced by the Kuraray Co., Ltd. As the matrix, a concrete composition typically employed in strain-hardening cement-based composites [59] was taken. The details concerning the fibers and matrix, as well as the results of pullout investigations of the interfacial behavior under quasi-static and high-rate loadings, were presented in [39]. Here, we will consider only quasi-static pullout tests (displacement rate of 0.01 µm/s) on as-received fibers with a mean diameter of 40 µm embedded in cylindrical concrete matrix "droplets" of diameter 2.6 mm. The diameter of each individual fiber was measured immediately after the pullout test by an optical microscope.

(2) E-glass fibers + Momentive RIM epoxy and a hemispherical geometry. The fibers, with a mean diameter of about 17 µm, were produced at the Leibniz-Institut für Polymerforschung Dresden e.V. (IPF) using a continuous pilot plant spinning equipment [60]. The matrix was an EPIKOTE™ Resin MGS™ RIMR135 epoxy/EPIKURE™ Curing Agent MGS™ RIMH137 hot-cure amino hardening system (manufactured by Momentive Specialty Chemicals), taken at the weight ratio 100:30, as recommended by the manufacturer. Individual fibers were embedded in hemispherical matrix droplets having a diameter of 2.5 µm (determined by the matrix holder) and then cured for 60 min at 85°C and postcured for 6 h at 80°C. A specialized single-fiber pullout testing apparatus, whose construction is described in detail in [61], was used to conduct quasi-static investigations at a displacement rate of 0.01 µm/s.

(3) Carbon fibers + Deyang poly(phenylene sulfide) (PPS) resin and a microbond test on small ellipsoidal matrix droplets. The microbond test was conducted by Liu et al. at the Sichuan University (China), and its results were reported in [62]. In this paper, we will consider their results as an example of microbond tests with ellipsoidal specimen geometry, because many researchers present only the general shape of force–displacement curves from the microbond test in their papers, and only these authors showed their experimental curve, with real force and displacement data. They used commercial T700SC-12000 carbon fibers (of diameter 7 µm) produced by Toray Co., Japan and a PPS resin with a melting temperature of 280°C, manufactured by Deyang Chemical Co. Ltd, Sichuan, China. The placing of matrix droplet on the fiber is described in detail in the original paper [62]. The droplet with the fiber inside was kept at 300°C for 1 min, then cooled down to ambient temperature

TABLE 2. Matrix Properties and Specimen Dimensions

Property	Matrices		
	Concrete	RIM R135/RIM H137 epoxy	Poly(phenylene sulfide)
Brand name (if applicable) and manufacturer	Portland cement + fly ash (see [39] for details)	Momentive Specialty Chemicals, USA RIM R135 resin RIM H137 hardener weight ratio 100:30	Deyang Chemical Co. Ltd., Sichuan, China
Conditions of specimens preparation	24 h at 23°C and RH = 50%, then 4 weeks at 23°C and RH = 90%	85°C/60 min, then 80°C/6 h	1 min at 300°C, then cooling down to room temperature and annealing at 120°C for 12 h
Radius of the matrix droplet R_m, mm	1.3 (cylindrical)	1.25 (hemispherical)	20-55 (small ellipsoidal droplets)
Tensile modulus E_m, GPa	28	3.0	4.5
Poisson's ratio v_{AM}	0.2	0.35	0.4
Stress-free temperature, °C	23	89	90
CTE a_m, 10^{-6} K^{-1}	—*	50	50

*If the stress-free temperature for a given fiber–matrix pair is equal to the test temperature, the coefficients of thermal expansion are not required for data evaluation.

and annealed in a vacuum oven at 120°C for 12 h. The microbond test was carried out using a special home-made apparatus at displacement rates from 1 to 150 μm/s.

The mechanical and thermal properties of the fibers and matrix required for calculating the interfacial strength parameters (τ_d and τ_f) are presented in Tables 1 and 2.

For each fiber–matrix pair, the values of τ_d and τ_f were determined using all the three methods described in Subsect. 1.6.

3. Results and Discussion

The values of τ_d and τ_f calculated for all the three fiber–matrix pairs investigated are presented in Table 3. In this Section, we will briefly discuss these results and point out the advantages and limitations of the methods used.

3.1. PVA fibers + concrete and a cylindrical specimen geometry

Figure 3a presents a typical force–displacement curve for this system (the inset shows its first part, i.e., the initial loading and debonding, on a larger scale). Evaluation of this curve by means of the methods described in Subsect. 1.6 yielded:

in the "traditional" approach, $\tau_{dt} = 31.33$ MPa and $\tau_{ft} = 1.44$ MPa;

in the "alternative" approach, $\tau_{da} = 38.55$ MPa and $\tau_{fa} = 1.08$ MPa.

Here, the subscript "t" stands for the "traditional" approach, and "a", for the "alternative" one. As can be seen, these pairs of parameters are rather close to each other. Some other force–displacement curves showed a greater difference between the values of τ_{dt} and τ_{da} for individual specimens, but the average values (over the set of 21 specimens) obtained by the "traditional" and "alternative" methods were nearly identical (see Table 3). Thus, it can be concluded that the mechanism of interfacial debonding in this system agrees well with the model described in Subsect. 1.4. We should note that the kink points were clearly discernible in all force–displacement curves, so that the debond forces could be measured easily. According to our experience, two main factors are responsible for a good discernibility of the kinks: (1) cylindrical specimen geometry and (2) great embedded length ($l_e \gg r_f$). It should be mentioned that the "indirect" method also yielded a very close value of τ_d for this system. At the same time, the value of the interfacial frictional stress obtained using this technique is not simply un-
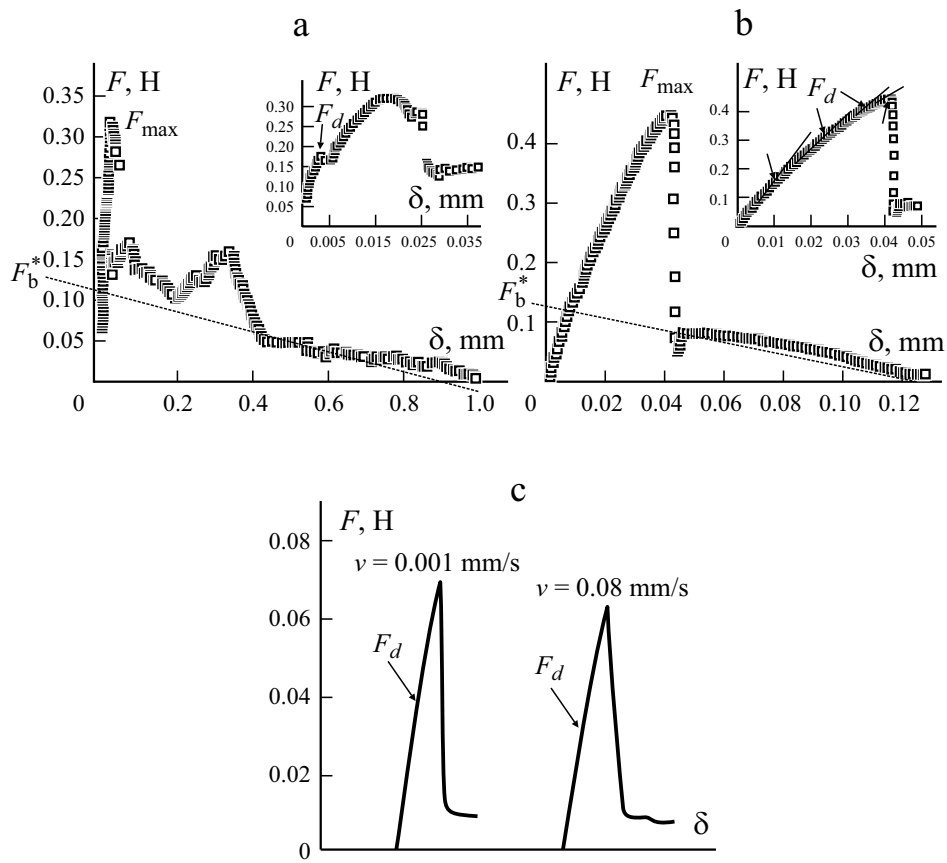
Fig. 3. Typical experimental force–displacement curves for PVA fibers–concrete, cylindrical geometry (a), E-glass–epoxy, hemispherical geometry (b), and carbon fiber–PPS resin, ellipsoidal geometry, microbond test [62] (c).

derestimated, but is very inaccurate. This is due to the fact that, in the case of a great embedded length, a small variation in τ_f or a great variation in τ_d may lead to comparable changes in the maximum force, $F_{\max}$ [15, 53]. Therefore, the indirect method can be recommended only when neither F_d nor F_b can be measured reliably [24].

3.2. E-glass fibers + Momentive RIM epoxy and a hemispherical geometry

Force–displacement curves for this fiber–matrix pair look quite different (Fig. 3b). The postdebonding "frictional" segment of the curve is fairly linear, and the interfacial frictional stress can be determined even more reliably than for the previous system. However, these curves have one disappointing feature: there are no a distinct kink in their growing part. Upon a more thorough investigation, it is seen see that the initial part of the curve consists of several complementary arched segments separated by points that can be considered as very indistinct kinks. For instance, four such "kinks" can be pointed out in the inset in Fig. 3b. The question is: does some of these points corresponds to crack initiation? And if so, which point is it?

To get the answer, we calculated the interfacial strength parameters τ_{dt} and τ_{ft} for all these points. Preliminarily, values of the local IFSS and the interfacial frictional stress were determined form this curve using the "alternative" approach in order to have a basis for comparison. These values were $\tau_{da} = 99.4$ MPa and $\tau_{fa} = 16.9$ MPa. The values of τ_{dt} and τ_{ft} obtained using the "traditional" approach, for all assumed kinks, are listed in Table 3. As expected, the calculated value of τ_{dt} increased with the accepted value of F_d. The behavior of the calculated value of τ_{ft} was also very interesting.

TABLE 3. Interfacial Strength Parameters (the Local IFSS τ_d and the Interfacial Frictional Stress τ_f) Calculated for Fiber–Matrix Systems Using Three Different Approaches.

Fiber	Matrix	Specimen geometry	Number of specimens	Approach	Local IFSS, MPa	Interfacial frictional stress, MPa
PVA	Concrete	Cylindrical	1	Traditional	31.3	1.44
			1	Alternative	38.6	1.08
			21	Traditional	29.7 ± 6.6	1.18 ± 1.01
			21	Alternative	29.5 ± 7.8	1.25 ± 0.98
			21	Indirect	29.8	0.60
Epoxy	E-glass Momentive	Hemispherical	1	Traditional[1]	26.8	Indeterminate*
			1	Traditional[2]	62.1	60.2
			1	Traditional[3]	84.9	49.6
			1	Traditional[4]	93.1	39.9
			1	Alternative	99.4	16.9
			12	Traditional[2]	57.3 ± 5.2	Indeterminate*
			12	Traditional[5]	82.9 ± 9.7	41.3 ± 8.0
			12	Alternative	92.3 ± 9.5	15.2 ± 2.2
			12	Indirect	92.1	0.00
Carbon	PPS	Ellipsoidal	1	Traditional[6]	59.9	46.1
			1	Alternative[6]	147.6	7.9
			26	Indirect[6]	89.5	40.9
			1	Traditional[7]	49.7	41.4
			1	Alternative[7]	135.5	6.3
			29	Indirect[7]	96.5	34.3

**The calculated τ_f is greater than τ_d, which is physically impossible.
[1]First kink, $F_d = 0.1275$ N
[2]Second kink, $F_d = 0.2949$ N
[3]Third kink, $F_d = 0.4032$ N
[4]Fourth kink, $F_d = 0.4423$ N
[5]Calculated using F_{max} from the last kink (3rd or 4th)
[6]Displacement rate of 0.001 mm/s
[7]Displacement rate of 0.08 mm/s

For the first kink ($F_d = 0.1275$ N), the calculated local IFSS was $\tau_{dt} = 26.8$ MPa. Attempts to calculate the frictional shear stress τ_{ft} using the traditional approach showed that the experimentally measured peak force $F_{max} = 0.4434$ N could be reached only if $\tau_{ft} > \tau_{dt}$! Since this is physically impossible (for this, F_b have to be greater than F_{max}), we concluded that the first kink did not correspond to crack initiation. The origin of this kink remains unclear. For instance, it cannot be attributed to a nonconstant IFSS along the embedded length, because this hypothesis does not explain the fact that almost all force–displacement curves had nearly the same number of kinks (3 or 4) at very close positions (F_d values). Another factor responsible for this kink could be a noncylindrical shape of specimen (for a droplet having the shape of a spherical segment, the fiber volume fraction rapidly decreases for deeper parts of the embedded fiber). As was demonstrated in [63], the kink position for such specimens is lower than for "equivalent cylinders." However, the specimen shape alone cannot generate multiple kinks!

For further kinks, the calculated values of τ_{ft} were smaller than the corresponding τ_{dt} and expectedly decreased with increase in the accepted values of F_d and τ_{dt}. However, as can be seen in Table 3, these values remain very high, much greater than the value of τ_{fa} reliably determined using the "alternative" approach. Only for the last (4th) kink, τ_{dt} is more or less close to τ_{da}, but, even in this case, the calculated τ_{ft} is more than twice greater than τ_{fa}. For the whole set of 12 specimens, even if we calculate interfacial strength parameters using the last kink, the value of τ_{ft} is greatly overestimated. We should also note that, for high values of F_d, a small variation in F_d causes a correspondingly small variation in τ_{dt}, but it drastically changes the calculated value of τ_{fa}, which points to great possible errors in the estimated interfacial frictional stress. Therefore, we consider the "alternative" approach as more reliable than the "traditional" method: at least, the values of τ_{fa} are accurate, and even errors in τ_{fa} cannot change the calculated value of τ_{da} considerably.

For this system, the "indirect" method yields a quite plausible (and close to τ_{da}) value of the local IFSS but, similarly to the previous fiber–matrix pair (Subsect. 3.1), it cannot give a reasonable estimate of τ_f.

3.3. Carbon fibers + PPS, microbond test, and ellipsoidal droplets

For this system, several plots of $F_{\max}$ versus the embedded length are given in [62] for different pullout rates, one force–displacement curve for each pullout rate. In our paper, we will consider the results of microbond test with pullout rates of 0.001 and 0.08 mm/s. The individual force–displacement curves are shown in Fig. 3c. In these curves, the values of $F_{\max}$ and F_b can easily be found. The positions of kinks are not very distinct, but measurable. As can be seen in Table 3, the difference between the results obtained using the "traditional" and "alternative" approaches is similar to that observed for the E-glass/epoxy system. The interfacial frictional stress calculated using the traditional approach is obviously greatly overestimated, and the values of τ_{dt} are correspondingly underestimated. On the other hand, the values of local IFSS from the "alternative" approach seem to be somewhat high. We could not evaluate all individual force–displacement curves, because they were unavailable; however, we had full information to use the indirect method for these specimen sets (26 specimens for the pullout rate of 0.001 mm/s and 29 specimens for 0.08 mm/s). The results appeared to be intermediate between those of the "traditional" and "alternative" approaches. As in previous Subsection, it can be expected that plausible are at least the values of local IFSS determined using the indirect method.

3.4. Comparison of all systems and outlook

Comparing all three examples of the microbond and pullout tests considered in this paper, we can conclude that the most important factor affecting test is specimen geometry. For cylindrical specimens, there was not found any significant difference between the values of interfacial strength parameters determined using three different methods of data reduction. For two other specimen shapes, the traditional approach obviously underestimates τ_d and overestimates τ_f, while the alternative method yields rather accurate values of τ_f and plausible values of τ_d. In part, this can be explained by the oversimplification in approximating the real specimen shapes by equivalent cylinders. Zhandarov and Mäder [64] simulated the force–displacement curves of pullout test with real-shape matrix droplets (including menisci) and found that, (1) for real-shaped specimens, the kink is rather smooth and its position cannot be found with full reliability, and (2) the kink force is smaller than the debond force in the equivalent cylinder, which results in a considerably underestimated value of the local IFSS if it is calculated using the equivalent cylinder approach. However, the alternative approach was not analyzed in their article. Moreover, they considered only model specimens with a priori known interfacial strength parameters τ_d and τ_f and did not suggest any procedure for determining these parameters from experimental force–displacement curves. The results presented in this paper clearly show the need for such a procedure. At present, we have made only the first steps in this direction [65]. Other factors that possibly affect the calculated value of local IFSS may be the inhomogeneous quality of interfacial bond (the local IFSS varies

not only from one specimen to another, but also along the interface in a given specimen) and the complex behavior of interfacial friction, which is very difficult to model.

Conclusion

The pullout and microbond tests are excellent techniques for investigating the interfacial strength in fiber–matrix systems, provided that an adequate method of raw data treatment is used. A comparison of three different approaches to data reduction has shown that the "alternative" approach, which uses the values of F_{max} and F_b, yields more reliable results than the "traditional" one, based on the debond force F_d, which often can be determined only with a great error. The evaluation of experimental data can be further improved if the real specimen shape is considered instead of the "equivalent cylinder" approximation.

REFERENCES

1. G. V. Shiriajeva and G. D. Andreevskaya, "Method of determination of the adhesion of resins to the surface of glass fibers," Plast. Massy, **4**, 42-43 (1962).
2. B. Miller, P. Muri, and L. Rebenfeld, "A microbond method for determination of the shear strength of a fiber–resin interface," Compos. Sci. Technol., **28**, 17-32 (1987).
3. L. S. Penn and E. R. Bowler, "A new approach to surface energy characterization for adhesive performance prediction," Surf. Interfac. Anal., **3**, 161-164 (1981).
4. E. Cailleux, T. Cutard, and G. Bernhart, Pullout of metallic fibres from a ceramic refractory matrix," Composites: Part A, **33**, 1461-1466 (2002).
5. W. Zhou, G. Yamamoto, Y. Fan, and A. Kawasaki, "In-situ characterization of interfacial shear strength in multi-walled carbon nanotube reinforced aluminum matrix composites," Carbon, **106**, 37-47 (2016).
6. W. P. Boshoff, V. Mechtcherine, and G. P. A. G. van Zijl, "Characterizing the time-dependant behavior on single fibre level of SHCC: Part 2: The rate effects on fibre pullout tests," Cement and Concrete Research, **39**, 787-797 (2009).
7. K. K. C. Ho, G. Kalinka, M. Q. Tran, N. V. Polyakova, and A. Bismarck, "Fluorinated carbon fibres and their suitability as reinforcement for fluoropolymers," Compos. Sci. Technol., **67**, 2699-2706 (2007).
8. R. V. Subramanian and K.-H. H. Shu, Silane coupling agents for basalt fiber reinforced polymer composites, in: Molecular Characterization of Composite Interfaces, ed. A. von Rubinowicz, Springer, pp. 205-236 (2013),
9. W. Liu, J. Huang, N. Wang, and S. Lei, "The influence of moisture content on the interfacial properties of natural palm fiber–matrix composite," Wood Sci. Technol., **49**, 371-387 (2015).
10. K. Tanaka, K. Minoshima, W. Grela, and K. Komai, "Characterization of te aramid/epoxy interfacial properties by means of pullout test and influence of water adsorption," Compos. Sci. Technol., **62**, 2169-2177 (2002).
11. A. Kelly and W. R. Tyson, "Tensile properties of fibre-reinforced metals: copper/tungsten and copper/molybdenum," J. Mech. Phys. Solid, **13**, 329-350 (1965).
12. Y. A. Gorbatkina, Adhesive Strength of Fiber-Polymer Systems, Ellis Horwood, New York, 1992.
13. G. Désarmot and J. P. Favre, "Advances in pullout testing and data analysis," Compos. Sci. Technol., **42**, 151-187 (1991).
14. N. Takeda, D. Y. Song, K. Nakata, and T. Shioya, "The effect of fiber surface treatment on the micro-fracture progress in glass fiber/Nylon 6 composites," Compos. Interfaces, **2**, 143-155 (1994).
15. S. Zhandarov and E. Mäder, "Peak force as function of the embedded length in the pullout and microbond tests: Effect of specimen geometry," J. Adhes. Sci. Technol., **19**, 817-855 (2005).
16. M. R. Piggott, "Why interface testing by single-fibre methods can be misleading," Compos. Sci. Technol., **57**, 965-974 (1997).
17. C. H. Liu and J. A. Nairn, "Analytical fracture mechanics of the microbond test including the effects of friction and thermal stresses," Int. J. Adhesion Adhesives, **19**, 59-70 (1999).

18. S. Zhandarov, E. Pisanova, and K. Schneider, "Fiber-stretching test: a new technique for characterizing the fiber–matrix interface using direct observation of crack initiation and propagation," J. Adhesion Sci. Technol., **14**, 381-398 (2000).

19. E. Pisanova, S. Zhandarov, E. Mäder, I. Ahmad, and R. J. Young, "Three techniques of interfacial bond strength estimation from direct observation of crack initiation and propagation in polymer–fibre systems," Composites: Part A, **32**, 435-443 (2001).

20. D. J. Bannister, M. C. Andrews, A. J. Cervenka, and R. J. Young, "Analysis of the single-fibre pullouttest by means of Raman spectroscopy: Part II. Micromechanics of deformation for an aramid/epoxy system," Compos. Sci. Technol., **53**, 411-421 (1995).

21. M. Shioya, E. Mikami, and T. Kikutani, "Analysis of single-fiber pullout from composites by using stress birefringence," Compos. Interfaces, **4**, 429-445 (1997).

22. R. J. Kerans and T. A. Parthasarathy, "Theoretical analysis of the fiber pullout and pushout tests," J. Am. Ceram. Soc., **74**, 1585-1596 (1991).

23. A. Hampe and C. Marotzke, "The energy release rate of the fiber/polymer matrix interface: measurement and theoretical analysis," J. Reinf. Plastics Compos., **16**, 341-352 (1997).

24. S. Zhandarov and E. Mäder, "An alternative method of determining the local interfacial shear strength from force–displacement curves in the pullout and microbond tests," Int. J. Adhesion Adhesives, **55**, 37-42 (2014).

25. S. F. Zhandarov, E. Mäder, and O. R. Yurkevich, "Indirect estimation of fiber/polymer bond strength and interfacial friction from maximum load values recorded in the microbond and pullout tests. Part I: Local bond strength," J. Adhes. Sci. Technol., **16**, 1171-1200 (2002).

26. L. B. Greszczuk, Theoretical studies of the mechanisms of the fibre–matrix interface. Interfaces in composites, ASTM STP 452. Philadelphia: American Society for Testing and Materials, 42-48 (1969).

27. J. P. Favre, G. Désarmot, O. Sudre, and A. Vassel, "Were McGarry or Shiriajeva right to measure glass–fiber adhesion?" Compos. Interfaces, **4**, 313-326 (1997).

28. T. Kanda and V. C. Li, „Interface property and apparent strength of high-strength hydrophilic fiber in cement matrix," J. Mater. Civil. Eng., **10**, 5-13 (1998).

29. C. K. Y. Leung and V. C. Li, "New strength-based model for the debonding of discontinuous fibers in an elastic matrix," J. Mater. Sci., **26**, 5996-6010 (1991).

30. S. J. Eichhorn, J. A. Bennett, Y. T. Shyng, R. J. Young, and R. J. Davies, "Analysis of interfacial micromechanics in microdroplet model composites using synchrotron microfocus X-ray diffraction," Compos. Sci. Technol., **66**, 2197-2205 (2006).

31. R. J. Scheer and J. A. Nairn, "Variational mechanics analysis of stresses and failure in microdrop debond specimens," Compos. Engineering, **2**, 641-654 (1992).

32. Y. C. Gao, Y. W. Mai, and B. Cotterell, "Fracture of fiber-reinforced materials," J. Appl. Mathem. Phys., **39**, 550-572 (1988).

33. H. Stang and S. P. Shah, "Failure of fiber reinforced composites by pullout fracture," J. Mater. Sci., **21**, 953-958 (1986).

34. C. K. Y. Leung, "Fracture-based two-way debonding model for discontinuous fibers in an elastic matrix," J. Eng. Mech., **118**, 2298-2318 (1992).

35. J. A. Nairn, "Analytical fracture mechanics analysis of the pullout test including the effects of friction and thermal stresses," Adv. Compos. Lett., **9**, 373-383 (2000).

36. S. Zhandarov, E. Pisanova, and B. Lauke, "Is there any contradiction between the stress and energy failure criteria in micromechanical tests? Part I. Crack initiation: stress-controlled or energy-controlled?" Compos. Interfaces, **5**, 387-404 (1998).

37. S. Zhandarov, E. Pisanova, and E. Mäder, "Is there any contradiction between the stress and energy failure criteria in micromechanical tests? Part III. Experimental observation of crack propagation in the microbond test," J. Adhesion Sci. Technol., **19**, 679-704 (2005).

38. W. Brameshuber and B. Banholzer, "Eine Methode zur Beschreibung des Verbundes zwischen Faser und zementgebundener Matrix, " Beton- und Stahlbetonbau, **96**, 663-669 (2001).

39. C. Scheffler, S. Zhandarov, W. Jenschke, and E. Mäder, "Poly (vinyl alcohol) fiber reinforced concrete: investigation of strain rate dependent interphase behavior with single fiber pullout test under quasi-static and high rate loading," J. Adhesion Sci. Technol., **27**, 385-402 (2013).

40. S. Radl, M. Kreimer, J. Manhart, T. Griesser, A. Moser, G. Pinter, G. Kalinka, W. Kern, and S. Schlögl, „Photocleavable epoxy based materials," Polymer, **69**, 159-168 (2015).

41. S. Meretz, W. Auersch, C. Marotzke, E. Schulz, and A. Hampe, "Investigation of morphology-dependent fracture behaviour with the single-fibre pullout test," Compos. Sci. Technol., **48**, 285-290 (1993).

42. I. Curosu, M. Liebscher, V. Mechtcherine, C. Bellmann, and S. Michel, "Tensile behavior of high-strength strain-hardening cement-based composites (HS-SHCC) made with high-performance polyethylene, aramid and PBO fibers," Cement and Concrete Research, **98**, 71-81 (2017).

43. M. Heppenstall-Butler, D. J. Bannister, and R. J. Young, "A study of transcrystalline polypropylene/single-aramid-fibre pullout behavior using Raman spectroscopy," Composites: Part A, **27**, 833-838 (1996).

44. P. Frantzis and R. Baggott, "Bond between reinforcing steel fibers and magnesium phosphate/calcium aluminate binders," Cement and Concrete Composites, **22**, 187-192 (2000).

45. P. Järvelä, K. W. Laitinen, J. Purola, and P. Törmälä, "The three-fibre method for measuring glass fibre to resin bond strength," Int. J. Adhesion Adhesives, **3**, 141-147 (1983).

46. S. Zhandarov, E. Pisanova, and E. Mäder, "Is there any contradiction between the stress and energy failure criteria in micromechanical tests? Part II. Crack propagation: Effect of friction on force–displacement curves," Compos. Interfaces, **7**, 149-175 (2000).

47. H. L. Cox, "The elasticity and strength of paper and other fibrous materials," Brit. J. Appl. Phys., **3**, 72-79 (1952).

48. A. H. Nayfeh, "Thermomechanically induced interfacial stresses in fibrous composites," Fibre Sci. Technol., **10**, 195-209 (1977).

49. J. A. Nairn, "Fracture mechanics of composites with residual thermal stresses," J. Appl. Mech., **64**, 804-810 (1997).

50. M. C. Andrews, D. J. Bannister, and R. J. Young, "Review: the interfacial properties of aramid/epoxy model composites," J. Mater. Sci., **31**, 3893-3913 (1996).

51. S. Zhandarov, E. Pisanova, E. Mäder, and J. A. Nairn, "Investigation of load transfer between the fiber and the matrix in pullout tests with fibers having different diameters," J. Adhes. Sci. Technol., **15**, 205-222 (2001).

52. S. Zhandarov and E. Mäder, "Characterization of fiber/matrix interface strength: applicability of different tests, approaches and parameters," Compos. Sci. Technol., **65**, 149-160 (2005).

53. S. Zhandarov and E. Mäder, "Indirect estimation of fiber/polymer bond strength and interfacial friction from maximum load values recorded in the microbond and pullout tests. Part II: Critical energy release rate," J. Adhes. Sci. Technol., **17**, 967-980 (2003).

54. B. J. Carroll, "The accurate measurement of contact angle, phase contact areas, drop volume, and Laplace excess pressure in drop-on-fiber systems," J. Colloid Interface Sci., **57**, 488-495 (1976).

55. R. J. Scheer and J. A. Nairn, "A comparison of several fracture mechanics methods for measuring interfacial toughness with microbond tests," J. Adhesion, **53**, 45-68 (1995).

56. R. W. Goettler and K. T. Faber, "Interfacial shear stresses in fiber-reinforced glasses," Compos. Sci. Technol., **37**, 129-147 (1989).

57. M. J. Pitkethly and J. B. Doble, "Characterizing the fibre/matrix interface of carbon fibre-reinforced composites using a single fibre pullout test," Composites: **21**, 389-395 (1990).

58. S. J. Park, M. K. Seo, H. Y. Kim, and D. R. Lee, "Studies on PAN-based carbon fibers irradiated by Ar+ ion beams," J. Colloid Interface Sci., **261**, 393-398 (2003).

59. P. H. Bischoff and S. H. Perry, Compressive behavior of concrete at high strain rates," Mater. Struct., **24**, 425-450 (1991).

60. W. Ehrentraut, R. Plonka, E. Mäder, and S. L. Gao, "Pilotanlage zum Erspinnen alkaliresistenter Glasfasern — Pilot equipment for continuous spinning of alkaline resistant glass fibers," Tech. Textilien/Technical Text., **48**, 22-24, E23-25 (2005).

61. E. Mäder, K. Grundke, H. J. Jacobasch, and G. Wachinger, "Surface, interphase and composite property relations in fibre-reinforced composites," Composites: **25**, 739-744 (1994).

62. B. Liu, Z. Liu, X. Wang, G. Zhang, S. Long, and J. Yang, "Interfacial shear strength of carbon fiber reinforced poly-phenylene sulfide measured by the microbond test," Polymer Testing, **32**, 724-730 (2013).

63. S. Zhandarov and E. Mäder, "Analysis of a pullout test with real specimen geometry. Part I: matrix droplet in the shape of a spherical segment," J. Adhesion Sci. Technol., **27**, 430-465 (2013).

64. S. Zhandarov and E. Mäder, "Analysis of a pullout test with real specimen geometry. Part II: the effect of meniscus," J. Adhesion Sci. Technol., **28**, 65-84 (2014).

65. S. Zhandarov and E. Mäder, "Alternative" method of pullouttest evaluation with real specimen geometry," Abstract book of PolyComTrib-2017: Int. Conf. on Polymer Composites and Tribology, Gomel (Belarus), June 27-30, 2017.